COMBINED USE OF POLAR ORBITING AND GEO-STATIONARY SATELLITES TO IMPROVE TIME INTERPOLATION IN DYNAMIC CROP MODELS FOR FOOD SECURITY ASSESSMENT

V. Venus [a, *], D. Rugege [b]

[a] Dept. of Natural Resources, International Institute for Geo-Information Science and Earth Observation (ITC), Hengelosestraat 99 P.O. Box 7500 AA Enschede, The Netherlands - venus@itc.nl
[b] RSA Centre for Environment and Development University of Natal, Pietermaritzburg Private Bag, X01 Scottsville 3209, South Africa - rugeged@nu.ac.za

Commission TS, WG VII/2 – Sustainable Agriculture & EcoSystem Approach

KEY WORDS: Remote Sensing, Agriculture, Monitoring, Temperature, Temporal, Multisensor

ABSTRACT:

Use of satellite data in crop growth monitoring could provide great value for regional food security assessments. By using the difference between remotely sensed crop canopy temperature and the corresponding ambient temperature at the time of the satellite overpass the daily actual rate of transpiration can be inferred. This relationship allows adjustment of the actual rate of assimilation and hence of actual crop growth. Although promising results were obtained using methods based on this premise, the sensitivity of these methods to temporal variability outside the time-window of the satellite overpass is a concern. Based on our findings we show that temporal aspects are indeed not negligible and an improvement in the accuracy of crop productivity assessments can be achieved if data from satellites with different temporal and spatial resolutions are combined. In this study, data from the *Advanced Very High Resolution Radiometers* (*AVHRR*) instrument aboard the polar orbiting satellite *National Oceanic and Atmospheric Administration #14* (*NOAA-14)* and data from the *Visible Infrared Spin Scan Radiometer* (*VISSR*) instrument onboard the *Geostationary Meteorological Satellite* #5 (*GMS-5*) are integrated in a dynamic crop growth simulation procedure. The existing estimation method we used to evaluate our results against solely dependents on data from polar orbiting satellites, which observe the earth surface too infrequently to yield sufficient clear-sky observations (only 24 out of 100 days of the crop cycle were cloud-free). More observations of temperature differences between the crop canopy and ambient air can be obtained when coupled with geo-stationary satellite measurements that represent the diurnal cycle. The linear interpolation procedure applied to obtain proxies for missing days improved accordingly. The results indicate that Storage Organ Mass (SOM) values can be determined from the new method with a higher degree of certainty as compared to the existing method. When evaluated against SOM values as observed at Quzhou, P.R. of China, experimental maize fields, the estimates are within an accuracy of about 150 kg ha^{-1}, a relative error of less than 1,8%. This also confirms our hypothesis that observations from geo-stationary satellites as an additional data source, which are more frequent available than measurements from polar orbiting satellites, can be useful to explain temporal dynamics of crop stress to better estimate regional crop productivity.

1. INTRODUCTION

1.1 Rational

Various approaches for estimating crop production have been proposed and tested since the 1960's to assist food (security) planners. These mainly aimed at improving traditional crop status reports and used techniques varying from crop growth simulation on a point-to-point basis to empirically derived index values that link satellite data with observed crop productivity. For regional applications, quantitative crop growth modeling is a most promising development since it considers the dynamics of essential physiological and environmental processes and thus aids in the universal quantification of productivity of food and fiber crops.

Observations from satellites have been found useful to infer the required parameters for crop growth modeling on a real-time and area basis, but procedures still remain challenging. Only few satellite sensors have a sufficient number of channels to derive input parameters meaningful for crop growth simulation.

Key to remotely sensed (RS) production estimation is the crop's energy budget. Incident solar radiation incident on the crop canopy is used in part for vaporization of water (crop transpiration). If less water is used (and assimilation and production are depressed) more energy is left for canopy heating, and vice versa. In other words, the difference between the remotely sensed crop canopy temperature and the corresponding ambient temperature is co-determined by the actual rate of crop transpiration. This temperature difference as detected at the moment of the satellite pass is then converted into daily equivalent values. If the transpiration term is isolated from the energy budget and divided by the theoretical transpiration rate of a constraint-free reference crop, a so-called 'coefficient of water sufficiency' with daily equivalent values (*cfH2O*, 0-1) results, indicating the degree stomata closure and therewith the degree to which photosynthetic activity is reduced by the compounded constraints to the actual crop. Recurrent reading at short intervals accounts for the dynamics of crop growth and produces successive, near real-time estimates of actual crop performance.

* Corresponding author.

However, in many cases data collection is hindered by the presence of clouds. This is particularly true for polar orbiting satellites; for only 24 out of 109 days of the crop cycle in 1999 it was possible to obtain cloud-free pixels from *NOAA-14* imagery to infer the crop performance as will be detailed shortly hereafter. Some scientists proposed interpretation techniques to overcome the temporal limitations of using satellite observations (Jin and Dickinson, 1999). Driessen and Rugege (2002) argued however that no interpretation procedure provides 'new' information; at best it reveals information that was hidden in the (collected and/or estimated) basic data and does so with varying accuracy. In this research we will try to (partly) alleviate this drawback by making use of multisensor satellite observations.

1.2 Objectives

The overall aim of this research is to develop knowledge and technology for crop production monitoring based on multi-sensor satellite data. The objective is to assess if an improvement in a crop production estimate can be obtained when the temporal resolution of parameter values are increased by combining data from satellites of different nature, to see if this enhances the detection of periods when the crop is subjected to stress.

2. METHODOLOGY: CROP GROWTH SIMULATION WITH RS-DATA

Analytical models of biophysical production potential of annual food and fiber crops have been built and tested in The Netherlands and elsewhere since the 1960's (De Wit and Penning de Vries, 1985). These models account for the dynamics of crop growth by dividing the crop cycle in successive (short) time intervals during which processes are assumed to take place at steady rates. 'State variables' such as leaf, root, stem and storage organ masses indicate the state of the system during a particular interval; their values are updated after each cycle of interval calculations. The relative simplicity and low data needs of these production situation analyses allow to accurately quantifying reference yield (i.e. the harvested produce) and production (i.e. total dry plant mass) levels, but for regional applications adequate basic data availability is a concern. As an adaptation from algorithms documented by Driessen and Konijn (1992), the crop growth simulation model (PSn) programmed for this research follows a similar line of reasoning but tries to improve upon its regional applicability by incorporating satellite derived parameter values.

2.1 Crop growth simulation

As a minimum configuration, known as 'Production Situation 1' (*PS-1*), the model represents a simplified Land Use System in which production and yield are solely determined by the available light, the temperature and the photosynthetic mechanism of the crop:

PS-1: P,Y = f(light, temperature, C3/C4) *(Eq.1)*

The levels of crop production and yield calculated for PS-1 are not the actual production and yield but potentials that are normally only realized at experiment stations where even the last weed plant or bug is mercilessly eliminated, irrespective of cost.

In many regions, water availability to the crop is the main constraint to crop growth. Water is needed in great quantity (in dry regions a maize crop may well transpire 1 cm of water on a clear sunny day, equivalent to 100,000 l $ha^{-1}d^{-1}$). Irrigation (and/or drainage) requires expensive infrastructure and skilled labour to restrict losses to the minimum and prevent soil degradation, e.g. caused by accumulation of soluble salts in the root zone. It has therefore been tried to extend the model with a water budget routine that matches actual consumptive water use with the crop's water requirement, i.e. with the theoretical transpiration rate of a constraint-free crop. The so-defined 'Production Situation 2' (*PS-2*) calculates the 'water-limited production potential' of the crop as a function of available light, temperature, photosynthetic mechanism and available water:

PS-2: P,Y = f(light, temperature, C3/C4, water) *(Eq.2)*

In production environments where the crop's consumptive water needs are met at all times, the water-limited production potential is equal to the biophysical production potential because actual crop transpiration is equal to the theoretical maximum rate. If water uptake by the roots is less than required to meet the maximum transpiration needs, actual transpiration is limited to the actual water uptake rate. In this case the 'water sufficiency coefficient' (*cfH2O*) assumes a value <1.0 and assimilation and growth are less than in Production Situation 1 due to water stress.

2.2 Crop stress and canopy heating

Incident radiation heats the canopy whereas transpiration cools it (Barros 1997; Kalluri and Townshed 1998). The fraction of the incoming radiation that is available for heating the canopy is set equal to the net intercepted radiation minus the energy needed for assimilation and for the vaporization of water lost in actual transpiration. The sensible heat component of the energy balance equation is approximated from the instantaneous temperature difference between air temperature and canopy temperature of a crop surface. More rigorous considerations of the momentum flux theory are provided by, inter alia, Bastiaanssen (1998) and Parodi (2000); isolated terms of the energy balance equations essential for this research are detailed below.

The latent heat flux can be isolated from the energy balance equation using a similar formulation as used by Soer (1980):

$$TRLOSS = (INTER) - \left(\frac{\Delta T * VHEATCAP}{AERODR} \right) \qquad (Eq.3)$$

TRLOSS represents the energy needed to vaporize the water lost in actual transpiration by the crop:

$$TRLOSS = TR_{act} * LATHEAT \qquad (Eq.4)$$

Where:
TR_{act} = is actual transpiration rate *[kg $m^{-2}s^{-1}$]*
LATHEAT = is latent heat of vaporisation *[2.46 * 10^6 J kg^{-1}]*

Isolating TR_{act} as a function of ΔT yields:

$$TR_{act} = \frac{INTER - \left(\frac{\Delta T * VHEATCAP}{AERODR} \right)}{LATHEAT} \qquad (Eq.5)$$

Introducing Equation 5 in crop growth simulation is only possible if parameter values are commensurate with the minimum temporal resolution of the simulation. The actual transpiration rate, TR_{act}, must be presented as a daily value, which implies that ΔT cannot be the instantaneous value measured at the time of the satellite pass but must be converted to an equivalent *daily* value.

The following procedure was adopted to obtain equivalent canopy temperature values for whole days (from instantaneous satellite observations):

- Calculate the equivalent satellite-derived instantaneous canopy temperature for days in-between measurements as a function of the daily rate of change over the interval between two successive cloud-free satellite observations in a linear interpolation procedure.
- Convert obtained instantaneous canopy temperatures to equivalent daily values by accounting for actual conditions during the day. To this end, the instantaneous canopy temperature values are multiplied by the fraction of sunshine hours for the day of year plus 20% of the clouded fraction. (It is assumed that there is still 20% radiation under an overcast sky.)

In the crop growth model, the equivalent daily canopy temperature for each day in the crop cycle is approximated with:

$$INTERTcan(adj.) = INTERTcan * CONVFAC \qquad (Eq.6)$$

Where:
INTERTcan = interpolated Satellite-derived temperature value *[°C]*
CONVFAC = conversion factor for actual daytime conditions.

With:
$$CONVFAC = (SUNH + 0.2 * (DL - SUNH)) / DL \qquad (Eq.7)$$

Equation 7 is applied to days with measurements as well as to days between measurements.

The *maximum* transpiration rate (TRmax) is a reference value conditioned by the evaporative demand of the atmosphere (represented by the potential water use from a Penman-type reference canopy) and the properties of the actual crop canopy, notably its exposure to the atmosphere:

$$TR_{max} = TR_0 * CFLEAF * TC \qquad (Eq.8)$$

Where:
TR_{max} = is maximum transpiration rate *[kg m^{-2} s^{-1}]*
TR_0 = is potential transpiration rate from Penman-type canopy *[kg m^{-2} s^{-1}]*
CFLEAF= is ground cover fraction of the actual canopy *[0-1]*
TC = is 'actual turbulence coefficient' *[-]*

The potential transpiration rate from a Penman-type canopy equals the potential evapotranspiration rate ($\boldsymbol{ET_0}$) minus the evaporation component ($\boldsymbol{E_{max}}$). The Penman-type reference canopy is defined as a short, green, closed, well-watered canopy with standard properties. The leaf area index (*LAI*) of this canopy will be close to *LAI* = 6 and the extinction coefficient is of the order of 0.5. It follows that the maximum rate of evaporation from underneath this reference canopy is approximated by $E_{max} = E_0 * exp(-ke * LAI) = E_0 * exp(-3) = 0.05 * E_0$. Consequently, potential transpiration from the reference canopy amounts to:

$$TR_0 = ET_0 - 0.05 * E_0 \qquad (Eq.9a)$$

Where:
ET_0 = is potential evapotranspiration rate from reference canopy *[kg m^{-2} s^{-1}]*
E_0 = is potential evaporation rate *[kg m^{-2} s^{-1}]*

If it is assumed that the difference between $\boldsymbol{ET_0}$ and $\boldsymbol{E_0}$ is small, i.e. within the error margin of satellite-derived $\boldsymbol{ET_0}$-estimates, $\boldsymbol{TR_0}$ can be approximated by:

$$TR_0 = 0.95 * ET_0 \qquad (Eq.9b)$$

The ground cover fraction of the actual crop canopy was described by equation 7. The effects of turbulence on the theoretical maximum transpiration rate are variable and complex; they depend on such diverse factors as wind speed, ET_0, canopy height, canopy roughness and parcel size. Driessen and Konijn (1992) propose a turbulence coefficient with values between 1.0 and a maximum coefficient value *TCM*. The value of *TCM* is set equal to the maximum value of the crop coefficient, kc, as defined by Doorenbos et al (1979). Driessen and Konijn (1992) suggest the following relationship:

$$TC = 1 + (TCM - 1) * CFLEAF \qquad (Eq.10)$$

With the sufficiency coefficient *cfH2O* equal to TR_{act} / TR_{max}, the parameter can thus be described as a function of the difference in temperature between the canopy and the surrounding air:

$$cfH2O = \left[\frac{INTER - \left(\frac{\Delta T * VHEATCAP}{AERODR} \right)}{LATHEAT * TRO * CFLEAF * TC} \right] \qquad (Eq.11)$$

On this basis, it becomes possible to adjust assimilation and calculated actual crop growth from instantaneous measurements or derivations of canopy and ambient temperatures. Note that the so obtained value of *cfH2O* takes the analysis beyond the water-limited production potential (PS-2 level) to the level of an actual-farmer (PS-n) without the necessity of accounting for all yield-limiting and yield-reducing factors (stress due to water scarcity, water logging, nutrient shortage or excesses, pests, diseases, pollutants etc). Stomatal closure due to water shortage is a well-documented and understood phenomenon. However, also pest and disease attacks on crops, depending on severity of the damage inflicted, reduce the numbers and/or the efficient functioning of stomata leading to reduced transpiration hence assimilation. The so-defined 'Production Situation n' (*PS-n*) calculates an 'actual-farmer's' production level of the crop as a function of available light, temperature, photosynthetic mechanism and compounded constraints (or crop stress) as reflected by the heating of the canopy:

PS-n: P,Y = f(light, temperature, C3/C4, canopy heating) (Eq.12)

Rugege and Driessen (2002) demonstrated that based on the same production function indeed highly accurate estimates of maize yield can be obtained. This has promise for regional applications since it greatly reduces the computational data needs with few other forcing variables needed then the

difference between ambient air and surface (or canopy) temperature. This is also the weakness of the approach that the uncertainty of the estimates increases when ΔT is not available for all days in the crop cycle, as often pixels are not entirely cloud-free at the moment of the satellite pass.

Note that for computations of ΔT the following is needed: one observer to record ambient air (T_a) and another for surface (or canopy) temperature (T_o). Key to accurately quantifying the thermodynamic process of transfer of energy from objects that are warmer than their surroundings to the air, or from the air to cooler objects, is that the absolute difference between the two are observed at the same instantaneous moment, and using observers that yield independent readings. Currently, ambient (air) temperature is often taken from meteorological surface observations. After these surface (point) observations have undergone objective analysis, their spatial and temporal resolutions have miraculously become commensurate with the surface (or skin) temperature observation from satellites. Diurnal variations of temperature (differences) can be highly dynamic, and in such cases the resulting *cfH2O* or any other derivation of the latent heat flux merely reflects the (lack of) quality of the interpolation technique being deployed rather than approximating the absolute transference of heat, inter alia crop stress. Even though acknowledged, for this research it is assumed that errors caused by this flaw can be neglected, and that positive differences between T_o and T_a can be fully subscribed to canopy heating, and thus crop stress. Maybe this is the proper moment to stress that this research is by no means perfect. As yet, no technique for inferring T_a from satellite data is available that provides estimates compliant with these requirements, i.e. that both parameters can be inferred from a single satellite using data observed at independent wavelengths, which as such would avoid any errors coming form the above mentioned viewing-time discrepancies.

2.2.1 Observing crop canopy heating from Space

A formidable challenge lies in combined use of data from multiple satellites of complementary specifications to further satisfy the spatial, temporal and radiometric requirements for canopy temperature inference. Estimating ambient air temperature from satellite data will possibly be dealt with in future experiments; this study focuses on estimating canopy temperature only.

2.2.2 Multi-sensor canopy temperature retrieval in retrospect: Accurate retrieval of surface temperature is complicated if measurements are made by sensors aboard satellite platforms far from the ground. Atmospheric attenuation processes including absorption, upward atmospheric radiance and bi-directional reflection of downward atmospheric radiance affect transmission of the emitted radiation. Absorption of water vapour is considered to be the most important factor influencing radiance transfer in the thermal spectral range (Bastiaanssen, 1995; Qin and Karnieli, 1999).

Polar orbiting satellites have a relatively high signal-to-noise ratio, and depending on the flight characteristics of the spacecraft in question they cover the same spot of the earth surface once every day. Coupled with cloudy conditions very few clear-sky satellite observations remain for repetitive skin temperature retrieval at a fixed position of the earth's sphere. For skin (or canopy) temperature inference the so-called 'split-window' technique is commonly applied for data from multi-thermal band sensors. The technique eliminates effects of water vapour absorption and emission by using data in the 10 to 13 μm range, often referred to as the T_{11} and T_{12} bands. The concept exploits the different absorption characteristics of the atmosphere within these different but close wavelengths, assuming that surface emissivity is constant over this spectral region. Detailed reviews of split-window algorithms are provided by Caselles et al (1997), Qin and Karnieli (1999) and by Parodi (2000).

Geo-stationary satellites observe diurnal changes of the atmosphere and earth surface, but due to their orbital height (approx. 30.000 km) at a lower signal-to-noise ratio. Despite their attractive temporal resolution they observe the earth surface at (nadir) resolutions of >5 km for TIR bands, actual resolutions depending on the sensor in question and distance from at nadir. Such spatial resolutions are insufficient for most regions, which have scattered land use practices resulting in mixed-pixel observations. Data from more *recent sensors with smaller at nadir resolutions (<3.25 km) may further help to overcome this drawback and permit to up scale the developed methodology to regions with less homogenous land cover. Most sensors aboard geo-stationary satellites also have two channels in the thermal infrared range of the spectrum (10 to 13 μm). Researchers have effectively exploited this to minimize the errors in estimating land surface (or canopy) temperature in a manner comparable to the split-window technique, as commonly applied to polar orbiting satellites data. In an attempt to further improve the technique for geo-stationary satellites. Sun and Pinker (2002) showed that by adding a second term of the brightness temperature difference $(T_{11}-T_{12})^2$, the atmospheric effect can be further removed. They also noted that when the satellite viewing angle increases, the optical path and the atmospheric attenuation increase also. After McClain et al. (1985) they added a zenith angle correction term ($sec\theta-1$) to further normalize the data for optical path variations. Yuichiroh (2004) further elaborated on this idea, and signalled that the effect of water vapor is not fully removed when the split-window technique is calibrated under general atmospheric conditions. After Coll and Caselles (1997) he attempted to further improve the algorithm by calculating various coefficients for different precipitable water levels (range: 0 – 5, precision: 0.01 (g/cm2)) using a radiative transfer model over *The Tibetan Plateau* for the application of the method to satellite data from *GMS-5*.

For this study satellite data from *NOAA-14* and *GMS-5* were used because of the similar specifications of the two instruments onboard these satellites and their complementary viewing frequency. The *NOAA-14* spacecraft passes at approx. 14.00 h local time (range: 13.00 – 15.00 h), whereas *GMS-5* scans the whole of South East Asia every hour.

---

* *SEVIRI* (*Spinning Enhanced Visible and Infra Red Imager*) instrument aboard the European geo-stationary *MSG-1* and *2* and the spectral channels of the Chinese *Visible and Infrared Spin Scan Radiometer* (*VISSR*) aboard the geo-stationary *FY-2C* will enhance upon the applicability of the procedures presented in this research by their improved temporal and spatial resolution.

2.2.3 Inter-calibration between GMS-5 and NOAA-14: Instrument calibrated data from *GMS-5* have been evaluated against calibrated data from the polar orbiting satellites *NOAA-14* by the Japanese Meteorological Satellite Center, JMA (Tokuno M., 1997). The results of their evaluation revealed that the brightness temperatures of *IR1* (10.5-11.5 µm) of *GMS-5* are about 1.2 (K) lower than those of *Ch4* (10.3-11.3 µm) of *NOAA-14/AVHRR* on average, and the brightness temperatures of *IR2* (11.5-12.5 µm) of *GMS-5/VISSR* are about 0.6 (K) higher than those of *Ch5* (11.5-12.5 µm) *NOAA-14/AVHRR*.

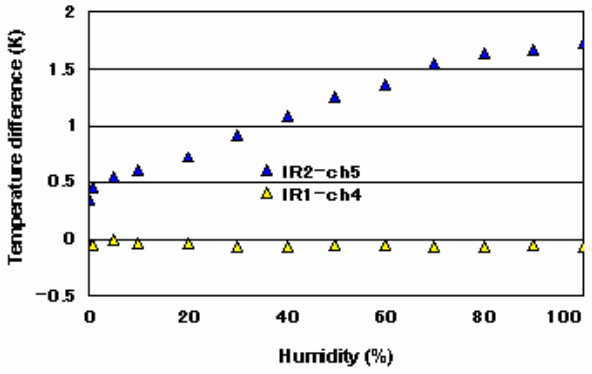

Figure 1. Influence of water vapour on differences in brightness temperatures for the *GMS-5/NOAA-14* split-window channels

Figure 1 shows the influence of water vapor by relating the brightness temperature difference for *IR1* vs. *Ch4* and *IR2* vs. *Ch5* at increasing levels of humidity. The sensitivity of *IR1* is almost the same as that of *Ch4*, whereas the sensitivity of *IR2* is greater than *Ch5* for higher humidity levels as can be seen form the increasing *IR2-Ch5* values. This is possibly caused by instrument differences between the two satellites.

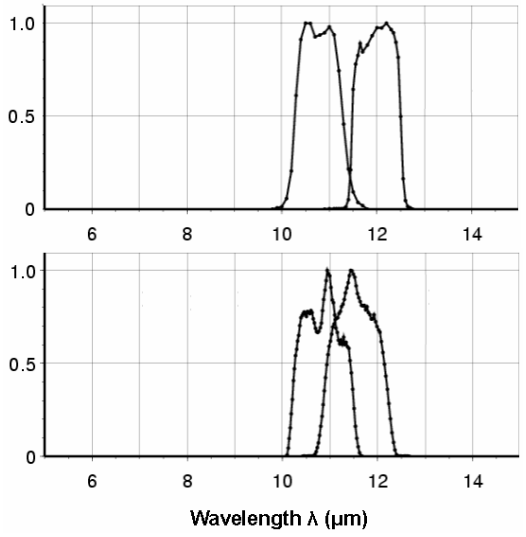

Figure 2. Instrument response curve for *NOAA-14/AVHRR* and *GMS-5/VISSR*

Figure 2 shows the normalized response curves (to a value of 1) of the two instruments as a function of wavelength after Yuichiroh (2004). Small, but apparently significant band-to-band wavelength and response function differences call for a careful selection of split-window algorithms for parallel land surface temperature retrieval, inter alia crop canopy temperature, from the two satellites.

2.2.4 Crop canopy temperature retrieval from GMS-5 and NOAA-14: The retrieval of canopy temperatures from satellite data is based on the Stephan-Boltzman black body emission equation:

$$R = \sigma \varepsilon_0 T^4 \qquad (Eq.13)$$

Where:
R = is radiation emitted by the surface (W m^{-2})
σ = 5.67 x 10^{-8} Wm^{-2} K^{-4} (the Stephan-Boltzman constant)
ε_0 = emissivity of the surface
T = surface temperature *[K]*

The emissivity term in the equation is a measure of the efficiency with which the surface emits energy. A perfect emitter, the black body, has an emissivity of 1. The black body is a theoretical concept whose behaviour does not exist in nature. The emissivity of most natural bodies lies between 0.91 and 0.98 in the thermal wave region 8-14 µm (Qin and Karnieli, 1999). Actual surface emissivity depends on surface characteristics such as the vegetation and the surface wetness, so that its diurnal variation is expected to be relatively small but day-to-day variation can be significant. We estimated the surface emissivity from *NOAA/AVHRR* visible channels by interpolating in-between days when *NOAA-14* observations were contaminated but *GMS-5* observations were cloud-free so temperature and emissivity separation was still needed. The procedure is the same as Kerr et al. (1992) and Sobrino et al. (2000), who estimated narrow-band emissivity semi-empirically from a *Normalized Difference Vegetation Index* (*NDVI*). The optical imagery from which this *NDVI* is computed are atmospherically corrected based on the *SMAC*–algorithm (Simplified Method for Atmospheric Correction of Satellite Measurements in the Solar Spectrum) using standard atmospheric conditions (Rahman, H., and G. Dedieu, 1994).

For observations from the polar-orbiting satellite the split-window algorithm developed by Coll and Caselles (1997) was selected to estimate maize crop canopy temperatures. The algorithm was selected based on the notion that it accounts better for water vapour then the split-window algorithm commonly applied, and because it has been calibrated for data from the two satellites used in this study. This in turn helps to improve to the consistency of the inference. This split-window algorithm takes the following form:

$$T_0 = c_1 \bullet (T11)^2 + c_2 \bullet T11 + c_3 \bullet T11 \bullet T12 + c_4 \bullet (T12)^2 + Offset \qquad (Eq.14)$$

Where:
T_0 = surface temperature [K]
$T11$, $T12$ = split-window brightness temperature [K]

The regression coefficient 'c_i' corrects for atmospheric water vapor; and the offset corrects for surface emissivity in bands *T11* and *T12*. For applications to the geo-stationary satellite the split-window algorithm takes the same form, except that the regression coefficient 'c_i' not only corrects for atmospheric water vapour but also accounts for the optical path length based on the satellite zenith angle. The algorithm was calibrated for *GMS-5* by Yuichiroh (2004) and used to estimate canopy temperatures in-between days *NOAA-14* observations were contaminated.

To derive land surface temperature it is essential to detect cloud-covered areas correctly because equation (14) is only available when the satellite receives radiation from the surface, and not from a cloud top. We utilized a cloud detection method which utilizes a combination of a semi-automated threshold brightness temperature *T11* filtering technique (unique for the two sensors) and a case-by-case analysis of the visible band, and in the case of GMS-5 also the water vapour band (*T6*, 6.7µm). Precipitable water (*PW)* was estimated by an empirical function using the *GMS-5/VISSR T6* band based on work by Chester et al. (1987).

2.2.5 Integration of Remotely Sensed Crop Canopy Temperature into the PS-n Model: Figure 3 below presents a relational diagram of the methodology for deriving canopy temperatures from satellite imagery and integrating them in the PS-n model by updating the temperature difference forcing variable. The flow diagram shows two parallel processes that feed data into the PS-n model. The right side of the flow diagram describes the canopy temperature retrieval process from satellite imagery using the split-window technique.

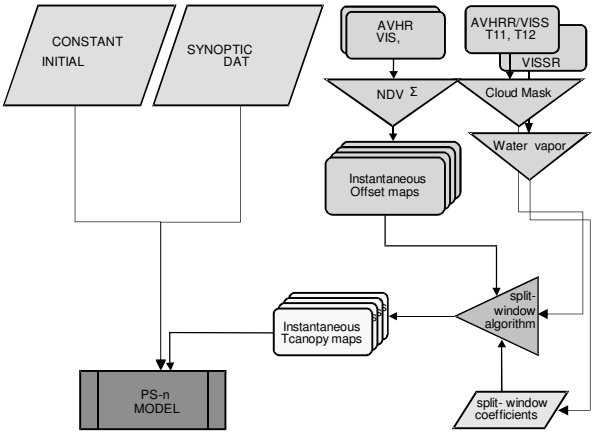

Figure 3. Relational diagram of the integration of satellite-derived crop canopy temperatures in the PS-n model

2.2.6 Data and study area: Satellite data for *GMS-5* were routinely processed and archived under the *GAME/Tibet* (*GEWEX Asian Monsoon Experiment*) project (Koike et al., 1999) and for the crop season of 1999 imagery was obtained through the Weather Satellite Image Archive as published by *Kochi University*, Japan (http://weather.is.kochi-u.ac.jp/archive-e.html). For the same period *NOAA/AVHRR* images, obtained from the *NOAA Satellite Active Archive* WWW site, were aggregated to the same pixel resolution of the *GMS-5/VISSR* TIR bands so they could be combined for our proposed multi-sensor crop production methodology. The table below shows the precision and value ranges of the satellite products, some of which are also depicted in Figure 3.

Map	Range	Precision
NDVI	-1 - 1	0.001
ε	0 - 1	0.001
PW	0 - 5	0.01
T_0	250 - 350	0.1

Table 1. Data precision and value ranges

To avoid mixed-land cover observations in one image pixel, a region characterized by homogeneous land cover and uniform soil characteristics was identified. The *North China Plain* consists of flat terrain at 40 m.a.s.l with uniform, re-washed loess (loam) soils. Located in these plains uniform Land Use Systems (>250 sq. km) were selected where experimental maize fields were set-up, within the administrative district Quzhou, People's Republic of China. Here, researchers from the *China Agricultural University*, Beijing routinely conduct the field trials, inter alia on maize production potentials. They kindly provided experimental production and yield data and correlated weather data recorded from an automatic recording station within the experimental site. In addition, planted areas and yields of surrounding administrative counties were provided for validation and calibration of the PS-n simulations.

3. RESULTS AND DISCUSSION

The results from the retrieval of canopy temperatures from satellite data from *GMS-5* and *NOAA-14* showed good internal agreement with a RMSE of 0.85, a BIAS of 0.92, and a STDV of 6.26 (Kelvin), as is also confirmed by the scatter plot of 37 observations as depicted in Figure 4.

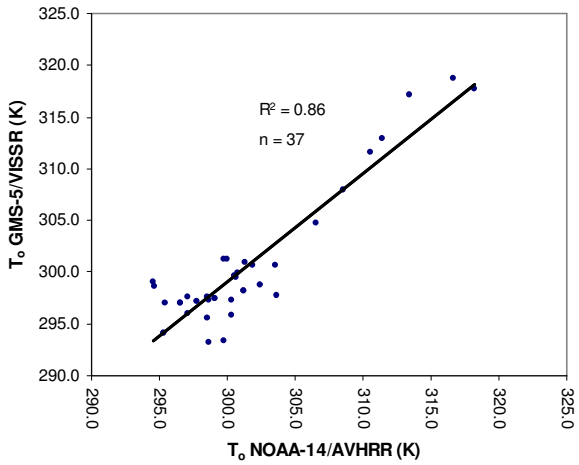

Figure 4. Scatter plot of estimated canopy temperature for *NOAA-14/AVHRR* and *GMS-5/VISSR*

As 'cloud-free' *AVHRR* imagery that could be obtained for the crop season of 1999 was not entirely free of cloud on all dates, selected pixels with no contamination were identified for further analysis. The PS-n model was run using canopy temperature data obtained from these selected pixels to update the 'TEMPDIFF' (*ΔT*) forcing variable including the pixel containing the Quzhou maize research site. As only 24 cloud-free *AVHRR* observations could obtained for the 1999 crop-season, it was necessary to fill in the days when canopy temperature data were unavailable. A linear interpolation procedure was applied conform the computational steps as detailed in section 2.2 of this paper (Eq.6 and 7) so as to obtain proxies for missing days. The upper part of Figure 5 shows the output curves of simulated (PS-n) structural plant matter development based on *NOAA-14/AVHRR* data alone. Crop stress indicated by the grey line (*cfH2O*) shows that the crop suffered from water shortage on multiple occasions. Specifically stress period 1a (*JD: 178 – 184) and 2a (JD: 262 – 265)

* Julian day

indicated by the vertical, light grey lines could very well be erroneous since the interpolation technique has to rely for its guess on relatively few observations. For its guess of the first stress period (1a) the technique relies on a single *NOAA-14* observation (JD: 182) of (temporal) canopy heating during a period of 21 days of no observations; only two observation of no crop stress preceded and proceeded (JD: 177 – 199). For estimating the second stress period (2a) the interpolation technique can rely on more *NOAA-14* observation (JD: 263, 264, 265). However, before the onset of this particular stress period (JD 262) there are again few observations available, with the last cloud-free satellite overpass occurring on JD 250. Hypothetically, the duration of crop stress could have been much longer if its onset was wrongly estimated merely due to a lack of observations.

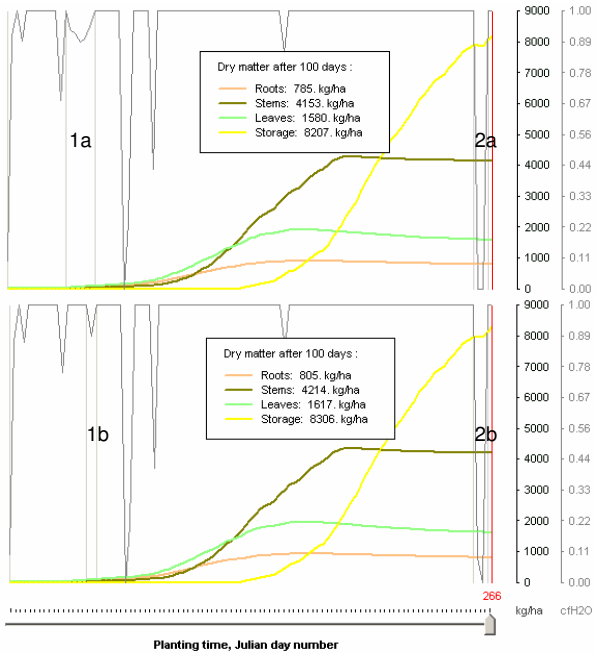

Figure 5. Dry matter growth curves simulated with the PS-n model on the basis of the canopy-ambient air temperature difference.

Since the time-window for obtaining satellite data based on the *NOAA-14* overpass ranges from 13.00 to 15.00 h, the introduction of *GMS-5* data theoretically triples our chances since the satellites scans our area of interest every hour (approx. 13.00, 14.00 and 15.00 h). With a bias towards obtaining additional cloud-free observations before, during and after these particular crop stress periods we were able to infer more ΔT values from *GMS-5*. Now 32 cloud-free observations could be used compared to only 24 out of 100 days of the crop cycle when we relied on data form *NOAA-14* alone. The robustness of the crop stress detection improved considerably, and seemed to confirm that the second period of stress (2a and 2b) was indeed as short as initially estimated. From five additional observations could be concluded there was indeed no canopy heating between JD 250 – 263. In addition, more observations during the first crop stress period could be obtained for days that were cloudy at the moment *NOAA-14* passed, but cloud-free just after or before this moment when *GMS-5* scanned our area of interest. The duration of the first stress period (1a) now proved to be much shorter (JD: 182 – 184 instead of 178 – 184) as indicated on the graph (1b), lower part of Figure 5.

The results indicate that Storage Organ Mass (SOM) values can be determined from the new method with a higher degree of certainty as compared to the existing method. When evaluated against SOM values as observed (8453 kg ha^{-1}) at Quzhou, P.R. of China, experimental maize fields, the estimates are within an accuracy of about 150 kg ha^{-1}, a relative error of less than 1.8%. This also confirms our hypothesis that observations from geo-stationary satellites as an additional data source, which are more frequently made than measurements from polar orbiting satellites, can be useful to explain temporal dynamics of crop stress to better estimate regional crop productivity.

REFERENCES

Bastiaanssen, W. G. M., 1995. Regionalization of surface flux densities and moisture indicators in composite terrain. Integrated Land, Soil and Water Research. PhD. -thesis. WAU, Wageningen, The Netherlands. 273 pp.

Bastiaanssen, W. G. M., 1998. A remote sensing surface energy balance algorithm for land (SEBAL). 1. Formulation. Journal of Hydrology: 212-214.

Barros, J. M., 1997. Quantitative Analysis of Selected Land-Use Systems. Ph.D.-thesis, WAU, Wageningen, The Netherlands. 169 pp.

Caselles, V., C. Coll and E. Valor, 1997. Land surface emissivity and temperature determination in the whole HAPEX-Sahel area from AVHRR data. International Journal of Remote Sensing, Vol. 18, No. 5:1009-1027.

Chester, D., W. D. Robmson and L. W. Uccellini (1987): Optimized retrievals of precipitable water from the VAS “Split windows”. J. Climate Appl. Meteor., 26, 1059–1066.

Doorenbos, J. et al, 1979. Yield Response to Water. FAO Irrigation and Drainage Paper 33. Rome. 193 pp.

Driessen, P.M., and N.T. Konijn, 1992. Land Use Systems Analysis. Wageningen Agricultural University, Wageningen, The Netherlands.

Driessen, P.M., and D. Rugege, 2002. Combining remote sensing and crop growth modeling for early warning applications, Innovative Soil-Plant Systems for Sustainable Agricultural Practices, 24.

Jin, M., and R. E. Dickinson, 1999. Interpolation of surface radiative temperature measured from polar orbiting satellites to a diurnal cycle, 1, Without clouds, J. Geophys. Res., 104, 2105-2116.

Kalluri, S. N. V. and J. R. G. Townshed, 1998. A Simple Single-layer Model to Estimate Transpiration from Vegetation using Multi-spectral and Meteorological Data. International Journal of Remote Sensing 19: 1037-1053.

Kerr, Y.H., Lagouarde, J. P., Imbernon, J., 1992. Accurate land surface temperature retrieval from AVHRR data with use of an improved split window algorithm. Remote Sensing of Environment. 1992. 41(2-3), pp 197-209.

Koike, T., Yasunari, T., Wang, J. and Yao, T., 1999. GAME-Tibet IOP Summary Report. In: *Proceeding of the 1st International Workshop on GAME-Tibet*, Xi'an, China, 1-2.

McClain, E. P., W. G. Pichel, and C. C. Walton, Comparative performance of AVHRR-based multichannel sea surface temperatures, J. Geophys. Res., 90 (C6), 11587-11601, 1985.

Parodi, G. N., 2000. AVHRR Hydrological Analysis System (AHAS). ITC Water Resources Division. Enschede, The Netherlands.

Qin, Z., and A. Karnieli, 1999. Progress in the remote sensing of land surface temperature and ground emissivity using NOAA-AVHRR data. Int. J. Remote Sensing 20, 12: 2367-2393.

Rahman, H., and G. Dedieu, 1994. SMAC : A Simplified Method for the Atmospheric Correction of Satellite Measurements in the Solar Spectrum. International Journal of Remote Sensing, vol 16, no. 1, 123-143.

Sobrino, J., A. and Raissouni, 2000. Towards remote sensing methods for land cover dynamic monitoring: application to Morocco. Int. J. Remote Sensing, 21, 353-366.

Sun, D. and R. T. Pinker, 2002. Estimation of Land Surface Temperature from a Geostationary Operational Environmental Satellite (GOES-8). *In revision for JGR–Atmospheres,* 2002.

Tokuno M., 1997. The Present and Future Calibration of Meteorological Satellite Sensors in Japan. In: *Proceedings of 1997 EUMETSAT Meteorological Satellite Data Users'* Conference pp. 615 - 622.

Wit, C. T. de and F.W.T. Penning de Vries, 1985. Predictive Models in Agricultural Production., Phil. Trans. R. Soc. London B310, London.

Yuichiroh, O., 2004. Estimation of Land Surface Temperature over the Tibetan Plateau. In: *American Meteorological Society 12th Conference Proceedings* Part 4.25, pp. unknown.